Rapid, open-source, and automated quantification of the head twitch response in C57BL/6J mice using DeepLabCut and Simple Behavioral Analysis

Alexander D. Maitland[1], Nicholas R. Gonzalez[1], Donna Walther[1], Francisco Pereira[2], Michael H. Baumann[1], and Grant C. Glatfelter[1*]

[1]Designer Drug Research Unit, National Institute on Drug Abuse, Intramural Research Program, Baltimore, Maryland

[2]Machine Learning Team, National Institute of Mental Health, Intramural Research Program, Bethesda, Maryland

*Corresponding author: grant.glatfelter@nih.gov

Abstract

Serotonergic psychedelics induce the head twitch response (HTR) in mice, an index of serotonin (5-HT) 2A receptor (5-HT_{2A}) agonism and a behavioral proxy for psychedelic effects in humans. Existing methods for detecting HTRs include time-consuming visual scoring, invasive magnetometer-based approaches, and analysis of videos using semi-automated commercial software. Here, we present a new automated approach for quantifying HTRs using the open-source machine learning-based toolkits, DeepLabCut (DLC) and Simple Behavioral Analysis (SimBA). First, pose estimation DLC models were trained to predict X,Y coordinates of 13 body parts of C57BL/6J mice using historical experimental videos of HTRs induced by various psychedelic drugs and experimental conditions. Next, a non-overlapping set of historical experimental videos was analyzed and used to train SimBA random forest behavioral classifiers to predict the presence of the HTR. The DLC+SimBA approach was then validated using a separate subset of visually scored videos. DLC+SimBA model performance was assessed at different video frame rates (120, 60, 30 frames per second or fps) and resolutions (50%, 25%, 12.5%). Our results indicate that HTRs can be quantified accurately at 120 fps and 50% resolution (precision = 95.45, recall = 95.56, F_1 = 95.51) or at lower frame rates (i.e., 60 fps and 50% resolution, precision = 91.00, recall = 86.23, F_1 = 88.55). The best performing DLC+SimBA model combination was deployed to evaluate the effects of bufotenine, a tryptamine derivative with uncharacterized potency and efficacy in the HTR paradigm. Interestingly, bufotenine only induced elevated HTRs (ED_{50} = 0.99 mg/kg, max counts = 24) when serotonin 1A receptors (5-HT_{1A}) were pharmacologically blocked. HTR scores for a subset of 21 videos from bufotenine experiments were strongly correlated across DLC+SimBA, visual review, and semi-automated software detection methods (r = 0.98 -0.99). In summary, the DLC+SimBA approach represents a rapid and accurate new method to detect HTRs from experimental video recordings using open-source toolkits.

Serotonin (5-HT) 2A receptor (5-HT_{2A}) agonists that induce psychedelic subjective effects in humans induce the head-twitch response (HTR) in mice, a rapid paroxysmal movement of the head.[1-4] The HTR is a reliable behavioral proxy of psychedelic drug effects in humans, with a strong positive correlation between drug potencies for HTR induction in C57Bl/6J mice and doses inducing subjective psychedelic activity in humans.[5] By providing a simple and reliable quantitative predictor of psychedelic-like drug effects, the mouse HTR has translational utility for examining the structure-activity relationships of serotonergic psychedelic compounds.[3]

Existing approaches for quantifying HTRs are effective but have limitations. Visual scoring of experimental video recordings is the simplest and most common approach for detecting HTRs and is often considered the "gold standard" for assessing accuracy of other methods of detection.[3, 6-11] However, visual scoring is time-consuming and requires multiple trained raters due to inter-individual variability in scoring and potential bias introduced by visual review. The HTR can also be quantified using magnetometer-based approaches, which involve detection of changes in coil voltage caused by a magnetic reporter surgically implanted on the skull or tags clipped on the ears.[1, 12-14] Magnetometer-based approaches allow for identification of a characteristic HTR wave form.[1, 13-15] More recently, automated methods employed machine learning (ML) approaches to extract HTRs from magnetometer recordings.[16]

Despite the high accuracy and rapid data collection of magnetometer-based approaches to measure HTR events, this strategy has some caveats. First, all current magnetometer-based methods require either surgical implantation of magnets on the skull or attachment of magnets to the ears. While ear magnets offer a less invasive alternative to surgery, Halberstadt (2020) noted that ear tags are difficult to maintain for extended periods and can be removed by cage mates.[16] Second, magnetometer setups are difficult to standardize given that the magnitude of the response depends on the physical dimensions of the coil and magnet size.[1, 17] A recent deployment and validation of the magnetometer-based detection system by Nakamura et al. [18] demonstrated high HTR detection accuracy (99%), but validation testing revealed a mean error detection rate of 11.20%. Third, novel compounds may produce unforeseen behaviors that increase false positive detection using magnetometer approaches.[13, 15, 16] In general, the behavioral effects of new pharmacological agents can be unpredictable, highlighting the advantage of video-based approaches which allow for manual review or assessment of behavioral effects of the drugs.

Video-based HTR detection in mice has been reported using several approaches.[1, 19] Glatfelter et al. [19] validated a semi-automated, commercial software-based method to detect the HTR from video recordings. This approach allows for rapid manual review of each time-stamped HTR event, but high-throughput drug screening is challenging due to lack of

automaticity and scalability. Furthermore, commercial software licenses may be prohibitively expensive for some laboratories. Therefore, there is a need to develop rapid, non-invasive, open-source, accurate, and fully automated HTR detection approaches based on the analysis of experimental video recordings. Machine learning-based behavioral analysis approaches for rodent behavior outperform commercial systems with human-level accuracy[20] and may present an improvement upon existing video-based HTR tracking strategies. In parallel to visual scoring, these approaches have also been reported in mice in addition to a comparable markerless deep learning algorithm approach to quantify HTR-like wet-dog shakes in rats.[21, 22] However, these approaches are limited in scope, detail, and validation assessments necessary for deployment in a drug discovery context.

To address these challenges, we developed a novel approach to characterize the HTR in mice using the open-source ML toolkits, DeepLabCut (DLC) and Simple Behavioral Analysis (SimBA). Using random historical experimental videos featuring HTR events across psychedelic chemotypes and experimental conditions, pose estimation data were extracted using DLC.[23, 24] The analysis time required to extract pose estimation data is a function of both the video resolution (how detailed the image is) and its frame rate (how smooth the video is). To allow evaluation of this trade-off, multiple models were trained using different video resolutions and frame rates to compare body part tracking performance and analysis speed. SimBA was then used to generate behavioral classifiers for the HTR for each combination of resolution and frame rate. Each DLC+SimBA model combination was then applied to a subset of 38 historical experimental videos, not used in training of DLC or SimBA models, to evaluate performance. To demonstrate the utility of the approach in psychedelic drug discovery, the best performing DLC+SimBA model combination was deployed to characterize bufotenine (5-hydroxy-*N*,*N*-dimethyltryptamine, 5-HO-DMT, or dimethylserotonin), a tryptamine derivative with purported psychedelic effects [25-29] and unknown potency and efficacy in the HTR paradigm. Overall, the present data show that our ML-based HTR detection tool is rapid, accurate, and can be used to create high-throughput workflows for preclinical assessment of psychedelic-like effects of compounds in drug development.

Results and Discussion

2.1 Mouse pose estimation model

Our previous studies with psychedelic drug administration in mice provided a rich library of historical videos depicting HTR events induced by various drug chemotypes under differing experimental conditions.[19, 30-34] This video library served as a source for model training, testing, and validation. For body part tracking of C57BL/6J mice, we used DLC [23, 24] and trained a model at each video resolution (50%, 25%, 12.5% of original video resolution). The 13 tracked body parts used for each pose estimation model are shown in **Figure 1A**.

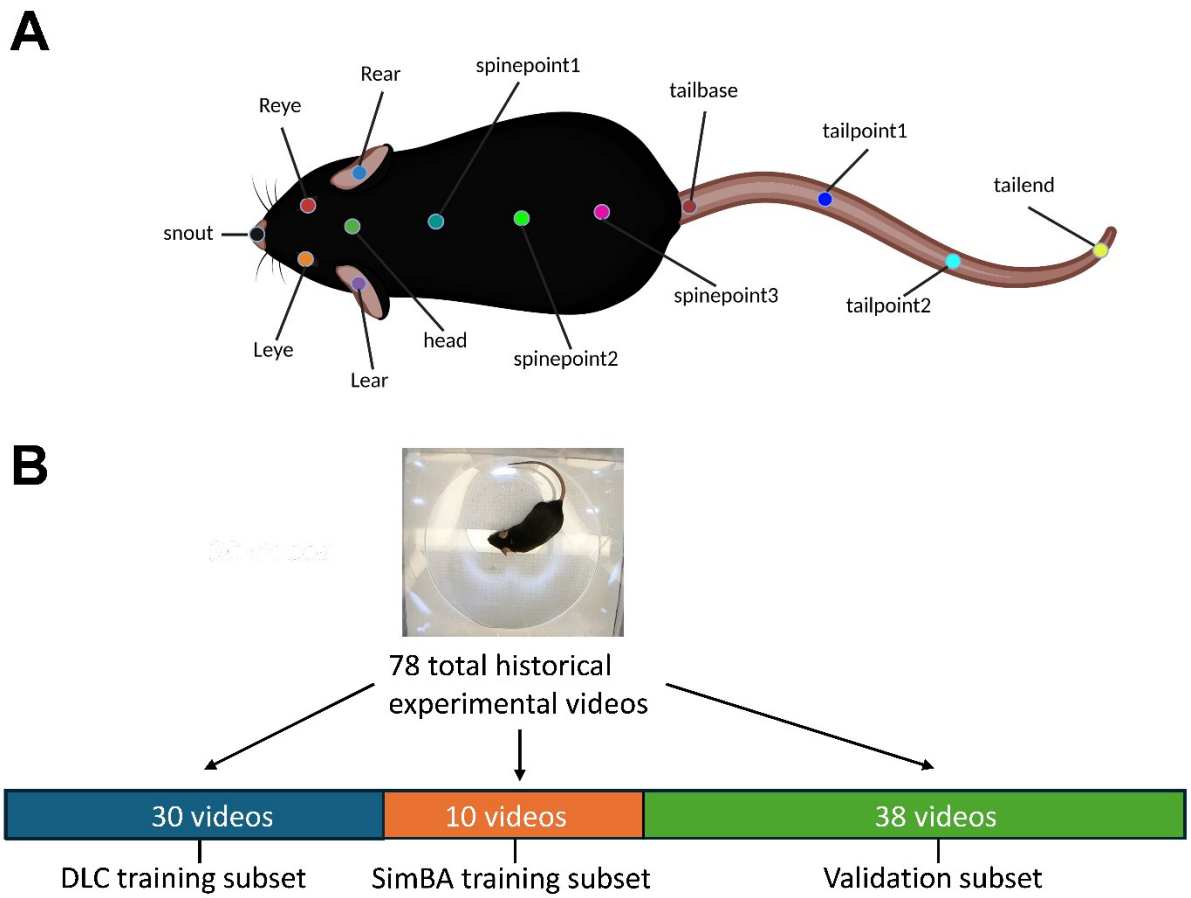

Figure. 1. C57BL/6J mouse body parts labeled for tracking (**A**) and schematic for processing of historical videos for HTR (**B**). All pose estimation models were trained to track the 13 body parts shown. Image for panel A was created in https://BioRender.com.

Specifically, extracted frames taken from 30 videos (at each resolution) and 16 animals (**Figure 1B**) were labeled. The final snapshot for each DLC model (computed root mean square error between the model-predicted labels and user labels) are shown in **Table S1**. Since each model was trained on the same set of videos, but at different resolutions, these are also reported as a percentage of the animal's body length to allow a direct comparison. These percentages suggest that the final DLC models trained at each video resolution were uniform in their body part tracking performance. Time cost for DLC model video analysis and FFmpeg video resolution downscaling for a subset of 10 experimental videos are reported in **Table S2**. Internal controls featuring an empty cylinder arena showed no animal tracking for any of the three DLC models (data not shown), and a historical experimental video featuring an immobile mouse featured consistent tracking for each of the three DLC models (data not shown). Visual inspection of labeled validation subset videos further confirmed model performance. As expected, the time cost for using FFmpeg and DLC

decreased in a frame rate- and resolution-dependent manner (**Table S2**). Overall time costs highlight that DLC+SimBA approach can rapidly quantify HTR, even at lower resolutions.

2.2 HTR behavioral classifier evaluation

After successfully training and validating pose estimation models, SimBA was used to generate 9 behavioral classifiers from a non-overlapping subset of 10 random historical experimental videos containing 136 HTR events (**Figure 1B**). Each of the 9 behavioral classifiers was then evaluated in a separate 'hold-out' validation subset containing 38 historical experimental video recordings, to assess the generalizability of each model combination (not included in the training or test set). Each classifier was evaluated in every frame of each of 38 historical experimental video recordings in the validation video subset, generating a prediction of whether a HTR event was present (positive) or not (negative). These predictions were compared against ground truth visually scored by three independent raters (r = 0.92 – 0.99, p < 0.0001). The scoring metrics calculated were the precision (true positives/all true and false positive events), recall (true positives/all true positive and false negative events), and F_1 scores (harmonic mean of precision and recall) across all the frames in the validation video subset (**Figure 2 & 3**). These validation videos included 18 experimental videos from Glatfelter et al. [19], and 20 additional random historical experimental videos across various psychedelic drugs (i.e. psilocybin, lysergic acid diethylamide or LSD, 2,5-dimethoxy-4-iodoamphetamine or DOI, 2,5-dimethoxy-4-butylamphetamine or DOBU, 2,5-dimethoxyamphetamine or 2,5-DMA, and 2,5-dimethoxy-4-propylamphetamine or DOPR), doses (0.001 – 30 mg/kg), lighting conditions (standard room overhead and enhanced lighting), and animals (male and female), for a total of 38 experimental videos (**Figure 1B**). Each of the 9 behavioral classifiers were assessed at various discrimination thresholds, from 0% to 50% (**Figure 2 & 3**).

Visual scores of the HTRs from three independent raters indicated the validation video subset contained 879 total HTR events. HTR classifier performance on the validation video subset decreased in a frame rate and resolution dependent manner, with high performance for each respective DLC+SimBA model combination at 120 fps irrespective of video resolution (F_1 = 95.51 - 83.40), with lower performance for 60 fps (F_1 = 88.55 - 63.72) and 30 fps (F_1 = 58.91 - 25.92) (**Figure 2 & 3, Figure S1**). Notably, the best performing 50% video resolution video and 60 fps model combination (F_1 = 88.55 at 0.35 discrimination threshold) outperformed the best performing 12.5% video resolution at 120 fps model (F_1 = 83.40 at 0.20 discrimination threshold), suggesting that high performance can be achieved even with lower resolution and frame rate videos. While not tested in the current study, training set construction in SimBA can influences F_1 score [35], and performance may further improve with more training videos containing HTR events. To account for variance in subjective annotations of HTR and further confirm the validity of these findings, we compared this performance to 9 behavioral classifiers annotated by another experimenter,

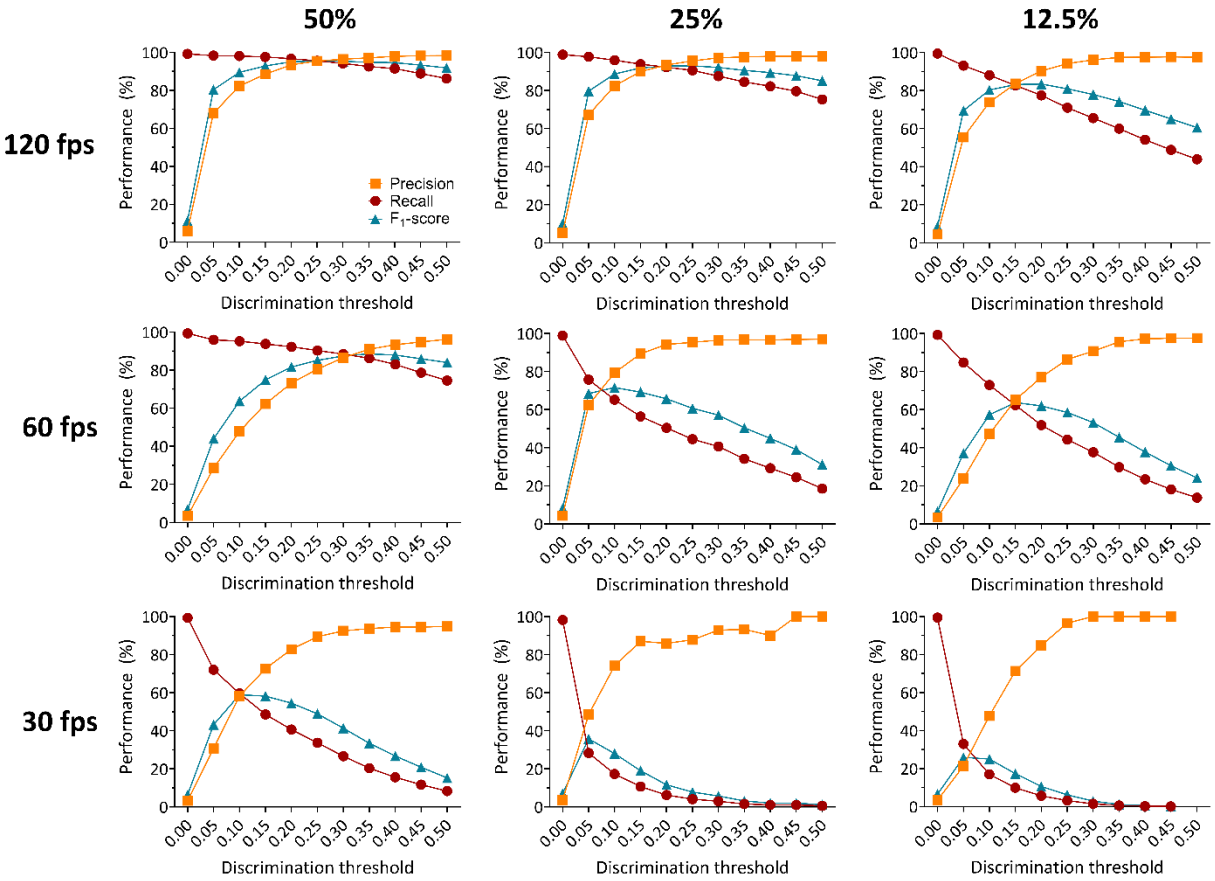

Figure 2. Accuracy-discrimination threshold curves for SimBA behavioral classifiers for 50%, 25%, and 12.5% video resolution at 120, 60, and 30 fps. Discrimination thresholds are the probability levels at which the behavioral classifier determines an HTR is detected. All minimum behavior bout lengths were set to 30 ms. Precision in red, recall in orange, and F_1 scores in teal at different discrimination thresholds are shown for all behavioral classifiers.

which produced similar accuracy-discrimination threshold curves and values (**Figure S2, Figure S3**). The patterns of performance as measured by best F_1 scores across DLC+SimBA model combinations were relatively indistinguishable, though optimal discrimination thresholds for HTR detection varied slightly (e.g. 0.25 to 0.30 at 50% resolution, 120 fps). Despite this, the overall performance similarities suggested that the performance of DLC+SimBA model combinations are similar between annotators.

As expected, performance reduced as video resolution and frame rate decreased. The best performing model combination, as measured by F_1 score, was the 50% resolution, 120 fps models at a discrimination threshold of 0.25. These results suggest that high frame rate video recordings are optimal for detecting the HTR behavior. For example, the 50%, 120 fps DLC+SimBA models at the 0.25 discrimination threshold featured a high precision (95.45) and recall (95.56), meaning that each HTR prediction had a 95% likelihood of correctly

identifying a true HTR, and these models captured 96% of all true HTR events in the validation video subset. Together, these findings support the deployment of this approach for automatic quantification of HTR events in experimental videos with moderate to high frame rates (i.e. 60 – 120 fps) and low to moderate scaled resolutions (25 – 50%) .

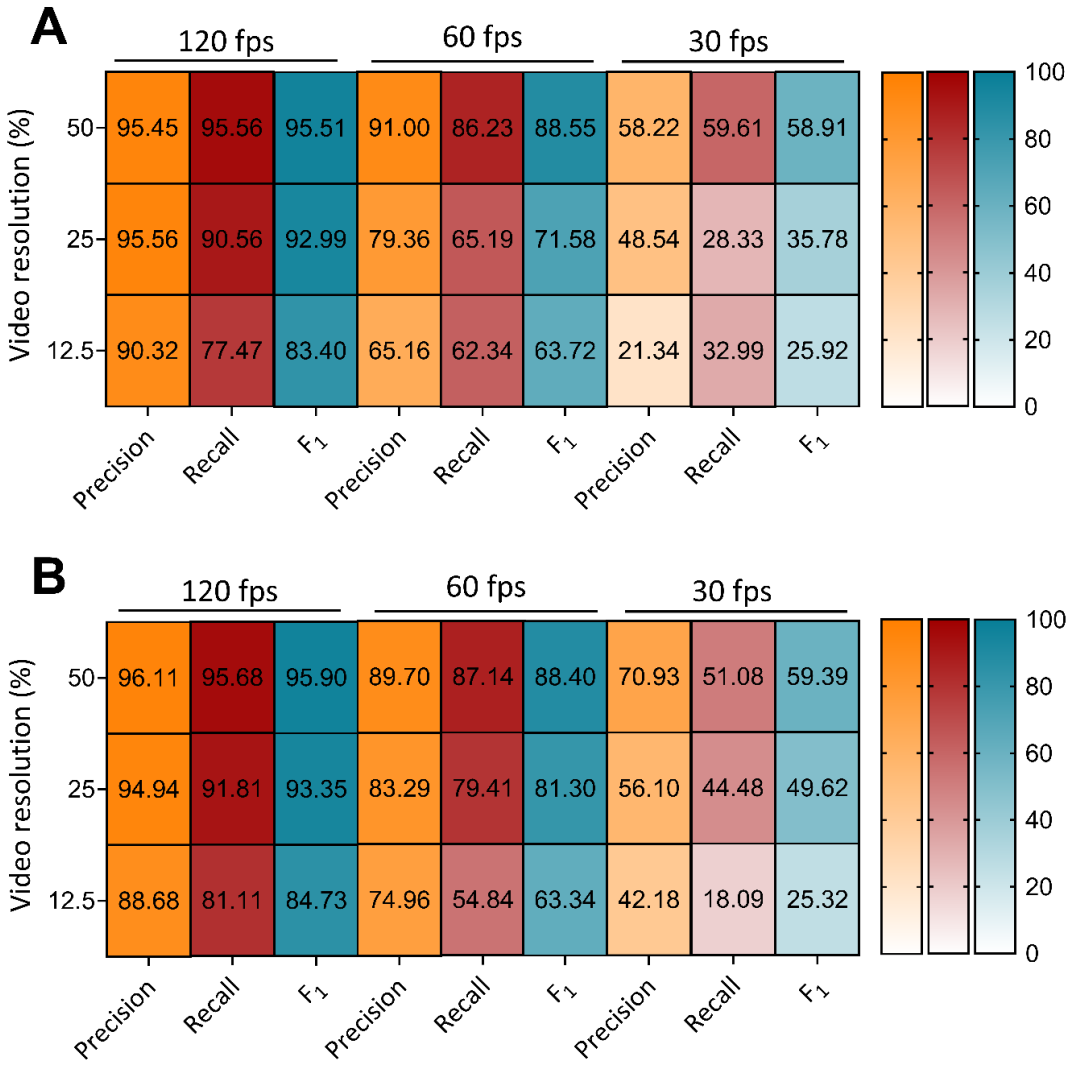

Figure 3. Heatmap visualization summarizing performance metrics at best performing accuracy-discrimination threshold for each SimBA classifier for 50%, 25%, and 12.5% video resolution at 120, 60, and 30 fps annotated originally (**A**) and by another experimenter (**B**). All minimum behavior bout lengths were set to 30 ms.

2.3 Post-hoc explainability metrics for HTR behavioral classifiers

A behavioral classifier produced with the SimBA toolkit makes its predictions based on the values of a set features tracked by DLC. In addition the prediction, SimBA also provides a quantitative measure of the importance of each feature to the prediction of the HTR behavior

by the classifier. For the specific classifier type used in SimBA, an ensemble model of decision trees, this is the mean decrease in impurity (also referred to as gini importance), a measure of the total decrease in node impurity averaged over all trees of the network/ensemble [36]. Averages for relative feature importances of each behavioral classifier at each resolution and frame rate were calculated for heatmap visualization (**Figure 4**). Based on mean decrease in impurity values, feature contributions were variable across classifiers, frame rates, and resolutions (range = 0.000428 – 0.132). This suggests that reliable tracking of some features may be affected by either of these factors, forcing classifiers to rely on other features with redundant or complementary information. Based on this metric, movement of the left ear (range = 0.0421 – 0.115), right ear (range = 0.0421 – 0.132), head (range = 0.0405 – 0.125), and first spine point labels (range = 0.0399 – 0.0994) were most important for predicting the HTR across all 120 fps and the 50%, 60 fps model combinations, with lower probability for detections among other features (range = 0.00043 – 0.0747).

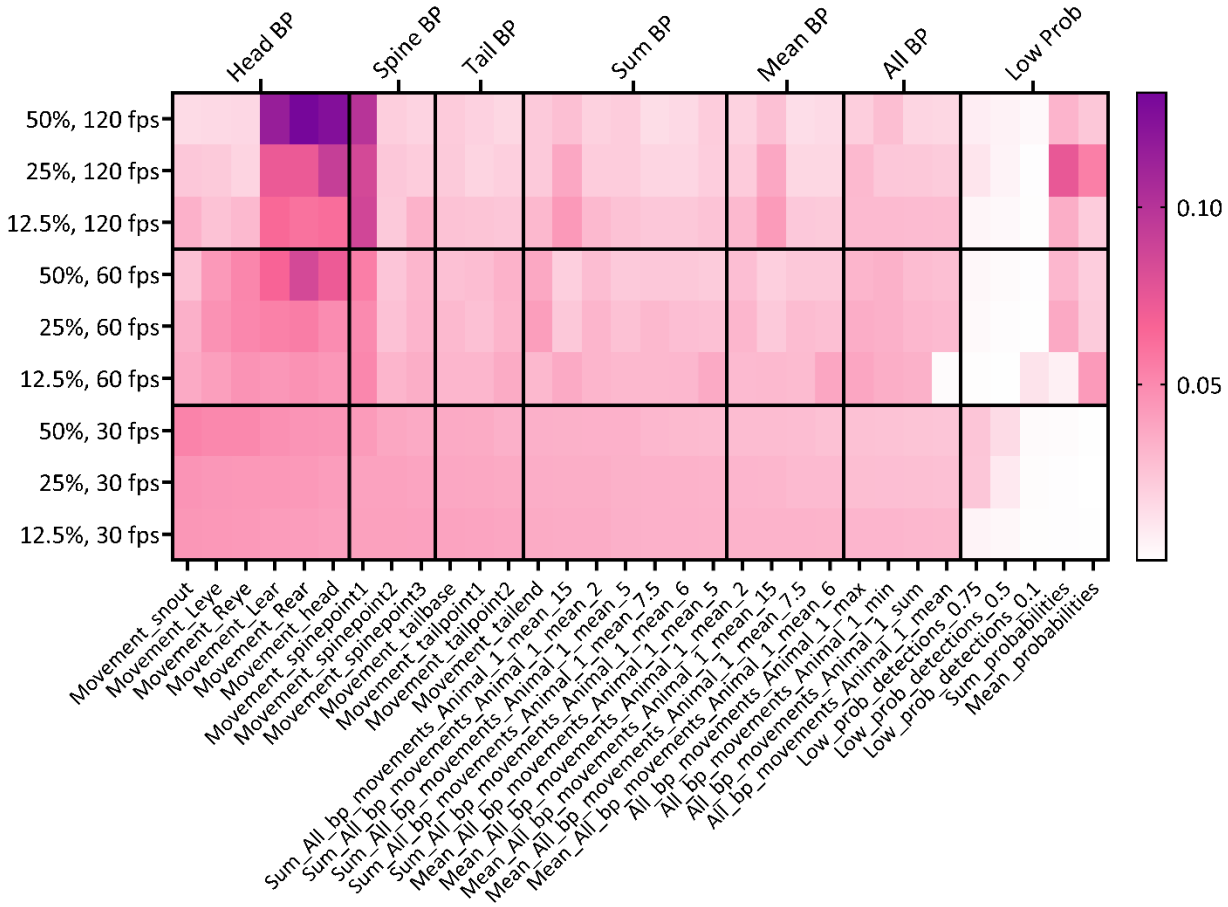

Figure 4. Feature importance as determined by mean decrease in impurity (gini importance) of all calculated features. The tile color corresponds to the relative importance value of each feature.

Relative importance of various categories was also visualized to further enhance interpretability by averaging related features (i.e. all features extracted from head body parts) (**Figure 4**). Head and upper-back body part movement features were the most important feature categories for the best performing model combinations across video resolutions at 120 fps as well as for the 50%, 60 fps model. Those feature categories were more important compared to the tail body part movement, all body part movement, and probabilities feature categories. The greater values for the head and upper-back features in these model combinations suggests a strong impact on predicting the HTR.

The feature importance indicates how much each feature contributes to the classifier prediction on average, across all the data that it was trained on. Beyond this, users may be interested in an explanation of which features contributed the most for the probability assigned to each behavior in a particular frame. For this purpose, SimBA provides Shapley Additive Explanations (SHAP), an explainability metric based on a game theoretic approach, which is particularly suitable for the random forest classifiers SimBA produces. SHAP analyses were conducted in SimBA on 100 random frames with HTR behavior present and 100 random frames with HTR behavior absent for each classifier, to measure the individual feature contributions to the overall frame behavior probability. In agreement with results using mean decrease in impurity, the Pearson correlations between each SHAP value sampled from frames where the behavior is present and absent show that features related to head and upper-back seem to substantially impact on HTR behavior probability for all resolutions at 120 fps as well as the 50%, 60 fps model (data not shown). For both post-hoc explainability metrics, the high importance of head and upper back-related body part movement features suggests these behavioral classifiers detect the HTR using body parts directly relevant to the HTR.

2.4 Behavioral control experiments using DLC+SimBA approach with SKF 38393-induced grooming and amphetamine-induced hyperlocomotion

The potential for false positive counts induced by competing behaviors (e.g. grooming, motor activity, jumping) are traditionally assessed in HTR detection method validation studies.[1, 13, 15, 16, 19] To further validate the DLC+SimBA approach, and compare present results to traditional HTR detection studies, the best performing model combination was tested for its ability to distinguish the HTR from grooming and hyperlocomotor activity.

The best performing models for HTR detection (50% resolution, 120 fps, F_1 = 95.51) were also deployed on downscaled historical experimental videos from Glatfelter et al. [19] examining SKF38393-induced grooming (12 videos) and d-amphetamine induced hyperlocomotion (16 videos) for a total of 28 videos. Using historical visual HTR scores from a trained independent rater, the performance, recall, and F_1 scores were evaluated (**Figure**

5). The behavioral classifier was assessed at various discrimination thresholds, from 0% to 95%. From these results, it was observed that the discrimination-accuracy curves were right-shifted compared to those obtained on the validation video subset. Practically, this means that higher discrimination thresholds would be required to obtain comparable measures of performance. Historical visual HTR scores indicated that these behavioral control videos contained 124 HTR events. At the best performing discrimination threshold of 0.25, the 50%, 120 fps models yielded greater false positives compared to the validation video subset evaluation (precision = 50.41) with very high recall (recall = 100). However, increasing the discrimination threshold to 60% reduced the number of false positives to levels (precision = 93.65, recall = 95.16, F_1 = 94.4) similar to the results from in the validation subset evaluation at 25% (precision = 95.45, recall = 95.56, F_1 = 95.51). Moreover, false positive detections decreased as the discrimination threshold increased beyond 60%, but at a greater cost to recall. Although there were few false positive detections at the 60% discrimination threshold (n = 8), several of these false positives occurred when the mouse turned its head while darting, or when rapidly rearing and turning its head.

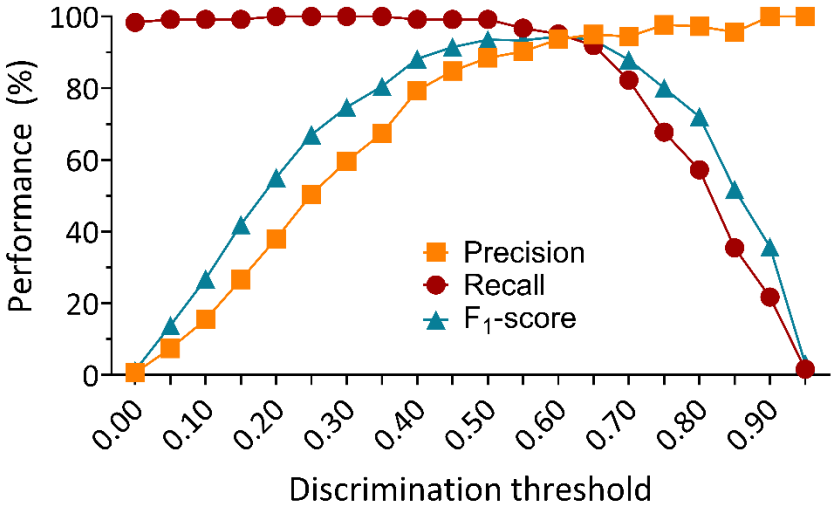

Figure 5. Accuracy-discrimination threshold curves using the 50% video resolution, 120 fps model combination for behavioral control videos. Discrimination thresholds are the probability levels at which the behavioral classifier determines an HTR is detected. All minimum behavior bout lengths were set to 30 ms.

Together, these findings indicate that the DLC+SimBA approach can reliably distinguish the HTR from similar behaviors, with performance equivalent to established automated HTR detection methods. By increasing the discrimination threshold, the detection of false positives was very low without sacrificing recall or precision, offering a viable strategy for addressing potential false positive counts. These findings further support the deployment of the DLC+SimBA approach for evaluating the HTR in a psychedelic drug discovery context.

2.5 Psychedelic-like effects of bufotenine using the DLC+SimBA HTR detection approach

To demonstrate the utility of our DLC+SimBA HTR detection approach in studying the psychedelic-like effects of 5-HT_{2A} agonists, the best performing model (50% resolution, 120 fps, F_1 = 95.51 for the 0.25 threshold) was deployed to characterize the HTR induced by bufotenine (5-HO-DMT or *N*,*N*-dimethylserotonin, **Figure 6A**). Bufotenine is a serotonergic psychedelic nonselective for 5-HT_{2A} with uncharacterized potency and efficacy in the HTR paradigm. A recent study in mice evaluated a 1 mg/kg dose of bufotenine administered intraperitoneally, finding ~20 – 30 HTRs [37], but a full dose-response evaluation was not conducted. Here, bufotenine was administered subcutaneously (s.c.) to mice at doses ranging from 0.03 to 30 mg/kg to measure acute effects of the drug on HTR, temperature change, and locomotor activity over a 30 min testing session.

Dose–response data for HTR induced by bufotenine over the testing session are shown in **Figure 6B** while time-course data are shown in **Figure S4A**. Descriptive statistics and additional details of statistical comparisons can be found in **Table S3**. Total HTR counts over the session for bufotenine were not significantly increased versus vehicle controls across the tested doses. However, compared to vehicle controls, bufotenine did induce small increases in HTRs from 0.1 – 1 mg/kg and decreases in HTR counts from 3 – 30 mg/kg (**Figure 6B**, **Figure S4A**). The typical inverted U dose-related effect seen for related tryptamines was evident for bufotenine, but the compound was judged to be inactive given small, negligible effects on HTR counts. Importantly, the descending limb of the HTR dose-response curve corresponded with doses inducing significant hypothermic and hypolocomotor effects relative to vehicle controls (**Figure 6C & D**, **Figure S5A**, **Table S3**), in agreement with existing literature for related tryptamines.[9, 30, 32-34, 38]

The weak HTR activity of bufotenine observed here is notable, given that its psychedelic-like effects appear to vary depending on the study, route of administration, and dose.[25-29, 39-42] Bufotenine is a natural product in plants and animals that has been used as part of snuffs or extracts in various cultures for its psychoactive and other effects.[26, 42-47] Like other serotonergic psychedelics, bufotenine interacts with 5-HT_{2A}, other 5-HT receptors (e.g. 5-HT_{1A}), and non-receptor sites of action (e.g. serotonin transporter or SERT).[48-55] 5-HT_{2A} mediates the primary psychedelic-like effects of serotonergic psychedelics related to bufotenine [2, 56-58], but non-5-HT_{2A} activities of the drugs, such as 5-HT_{1A} and SERT, can inhibit expression of the HTR of some compounds as well as their subjective effects in humans.[31-33, 38, 59-66]

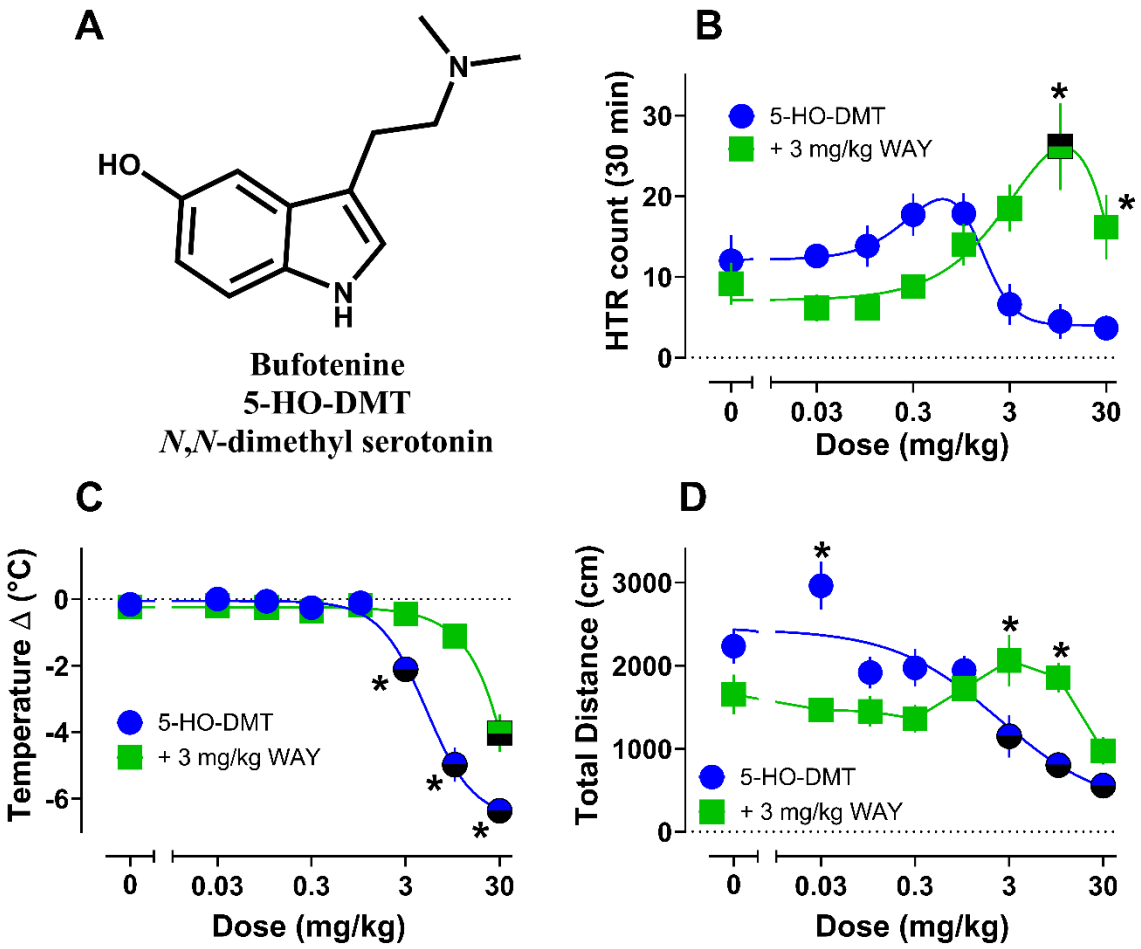

Figure 6. Dose-response curves for effects of bufotenine without and with WAY100635 pretreatment on HTR. (**A**) the freebase chemical structure of bufotenine. All experimental videos were analyzed using the 50%, 120 fps model DLC+SimBA combination at 0.25 discrimination threshold for HTR counts (**B**), body temperature change pre vs post session (**C**), and total distance traveled during the 30 min testing period (**D**). All values are mean ± SEM and represent n = 5 – 7 mice per data point. Half bolded symbols represent statistical differences from vehicle controls for each group, while asterisks represent statistical differences between groups across doses ($p < 0.05$).

Given that compounds with pharmacological profiles like bufotenine can be "false negatives" in the HTR paradigm [32, 59], we sought to evaluate the role of 5-HT$_{1A}$ in modulation of the HTR by the drug, especially since it displayed a biphasic dose-response curve for induction of HTR (**Figure 6B**) and induces psychedelic subjective effects in humans in some contexts.[26, 27, 41, 43] Mice were pretreated with the 5-HT$_{1A}$ antagonist WAY100635 (3 mg/kg sc.) 10 mins prior to administration of bufotenine (0 – 30 mg/kg sc.), and acute effects on HTR, body temp, and motor activity were measured for 30 min. Pretreatment with WAY100635 revealed a more pronounced HTR curve, with significantly elevated counts vs. vehicle controls at 10 mg/kg (**Figure 6B**, **Table S3**). The potency and efficacy for bufotenine to induce the HTR under

these conditions (ED_{50} = 0.99 mg/kg , E_{max} = 24 counts) were similar to the results obtained with 5-methoxy-*N*,*N*-dimethyltryptamine (5-MeO-DMT) analogs and WAY100635 pretreatment.[32] Corresponding with the more pronounced HTR, bufotenine+WAY100635 treatment also blocked hypothermic and hypolocomotor effects except at the highest dose (30 mg/kg, **Figure 6C & D**, **Table S3**). Time-course plots for HTRs and motor activity across the 30 min session in WAY100635 pretreatment experiments are shown in **Figure S4B** & **Figure S5B**, showing that only the highest dose had a delayed (~10-15 min post bufotenine) effect to reduce motor activity and HTR counts.

Despite the greater HTR activity produced by bufotenine plus 5-HT_{1A} blockade, the compound was still weaker in potency and efficacy compared to related compounds such as psilocin (ED_{50} = 0.11 – 0.17 mg/kg, E_{max} = ~23) and *N*,*N*-dimethyltryptamine (DMT; ED_{50} = 1.54 mg/kg, E_{max} = ~76).[5, 34] The reduced activity of bufotenine could be due to several factors such as poor blood brain barrier penetration, rapid metabolism, route of administration, other pharmacological activities (i.e. SERT), or a combination thereof.[26-29, 39, 42, 48, 67, 68] Prior studies show that bufotenine is a potent substrate-type releaser at SERT [48], which may impact its pharmacological effects. Here, we also studied the monoamine transporter activity of bufotenine using rat brain synaptosome preparations. Consistent with previous data [48], bufotenine was a selective and potent SERT releasing agent (SERT release EC_{50} = 97 nM) comparable to the entactogen, 3,4-methylenedioxymethamphetamine (MDMA; SERT release EC_{50} = 81 nM; **Figure S6A - C**). Given that the pharmacological effects of other serotonergic psychedelics, such as psilocybin and LSD, are influenced by SERT activity [62-64, 66], it seems possible that SERT substrate actions of bufotenine may influence its ability to elicit the HTR. Notably, HTR counts at low doses (i.e. 0.03 – 0.1) of bufotenine in the presence of WAY100635 were lower relative to bufotenine alone. This suggests that blockade of 5-HT_{1A} receptors in the presence of bufotenine may enhance non-selective 5-HT receptor signaling from SERT-mediated 5-HT release and reduce HTR counts indirectly.

2.5 Comparing DLC+SimBA vs. visual and commercial software-based HTR detection approaches

A subset of 21 videos randomly chosen across doses/treatments from the bufotenine dose-response and WAY100635 antagonist pretreatment studies were next visually scored by an experimenter blind to drug treatments. These videos were also scored using the semi-automated commercially available approach utilizing the TopScan software platform (Clever Sys Inc.) previously validated in our laboratory.[19] Scores from these approaches were then compared to scores from the best performing DLC+SimBA model combination. Visual scoring results revealed that there were 326 total HTR events recorded across the 21 videos (11 bufotenine and 10 bufotenine + WAY), while the DLC+SimBA model (50%, 120 fps, 0.25 discrimination threshold) found slightly higher overall counts (331, 102% of visual) and the

commercial software method found lower HTR counts (284, 87% of visual). Values from all 3 data sets were strongly correlated (**Figure 7A – C**), supporting similarity of the values across scoring methods. Importantly, all of the discrepancies in counts on a video-to-video level were ≤ 6 counts (mean difference between methods = ~2), which likely is within the margin of inter-rater variability error seen with averaging visual scores from multiple raters.[1, 69] When manually reviewing extra events scored by the DLC+SimBA approach vs. visual scoring, it was noted that some of the scored events were missed visually, hence the results featured slightly higher counts than with visual scoring.

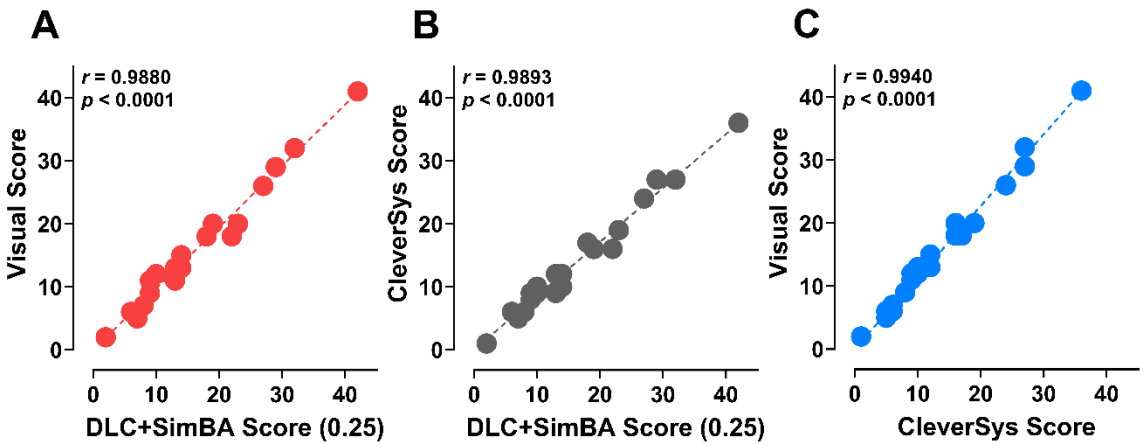

Figure 7. Correlations between HTR counts from 21 videos (bufotenine and WAY+bufotenine) across detection methods. (**A**) DLC+SimBA vs. visual scores, (**B**) commercial software vs. DLC+SimBA scores, and (**C**) visual scoring vs. commercial software scores.

2.6 Advantages and limitations of using DLC + SimBA for HTR detection vs. other approaches

Here, we develop, validate, and deploy the deep learning-based pose estimation toolkit DLC and the behavioral classifier toolkit SimBA to demonstrate its utility as a rapid, accurate, and open-source approach to examine the behavioral effects of 5-HT_{2A} activity. The present approach has several key advantages over existing software-based approaches to HTR detection [19], while overcoming potential limitations of magnetometer and existing software-based approaches.

Visual scoring of the HTR is time-consuming, typically requires multiple trained raters, and can exhibit inter-rater variability in scores.[1, 69] While quantification of HTRs has been reported using commercial software [19] and ML approaches [21, 22], the present approach is the first to automate and validate this process with experimental videos in mice. Results from our best performing models suggest similar or improved performance metrics compared to the best performing DLC+SimBA model in the Cyrano and Popik [22] study in rats. However,

the approaches are not directly comparable as the prior study focused on tracking the facial movements of rats from both sides of a cage, and rat wet-dog shakes have not been validated for predicting potency for psychedelic-like effects of drugs in humans. The only animal models that have been validated to predict potencies of psychedelics to induce subject effects in humans are drug discrimination in rats and the HTR paradigm in C57BL/6J mice.[5] Furthermore, rats do not respond the same across classes of psychedelics compared to C57BL/6J mice. For instance, the tryptamine psychedelics, psilocybin and DMT, produce measurable HTR in C57BL/6J mice [5, 34, 70], but these drugs do not elicit appreciable wet-dog shakes in Sprague Dawley rats (Pego et al. 2025 in review, Baumann et al. 2025 in review; [71]), which respond robustly to phenethylamine psychedelics for this endpoint.[72] Therefore, validation of the DLC+SimBA approach for studying the HTR in mice is an important advancement of available detection methods.

By comparison across HTR detection methods, accuracy for the semi-automated software-based approach from Glatfelter et al. [19] was found to be 86 - 94% (depending on lighting conditions), which is slightly lower than values reported for magnetometer-based systems (96% - 99%) and the present approach (102%). Notably, the DLC+SimBA HTR scores were elevated due to a small number of true positive events missed by visual raters. Regardless of these differences, software- and magnetometer-based approaches generally agree on HTR potencies and relative maximal values observed across studies.[5, 34, 73, 74] However, accuracy measures alone may be insufficient for evaluating the robustness of an HTR detection method. A recent performance assessment of the modern magnetometer approach described originally by Halberstadt and Geyer [1] provided information regarding the number of HTR counts, false positives, and false negatives.[18] From the study results (see Table 1)[18], the best calculated F_1 score was ~95%, comparable to the F_1 score in our best performing model combination (96%) at 50% video resolution, 120 fps. Together, our results suggest that our DLC+SimBA HTR detection approach exhibits equivalent or greater performance compared to published assessments of other approaches.

In addition to excellent HTR detection, our ML video recording-based approach overcomes several disadvantages of magnetometer setups. First, all existing magnetometer-based methods require intracranial surgery for head magnet implantation or anesthesia for ear-tag placement. Head-mounted magnets can reportedly detach from the skull via removal by an animal or cage mates if group housed [75], and ear-tag magnets can damage the ears and are difficult to maintain for long periods of time.[5, 15] Video-based approaches are non-invasive and do not require surgery by comparison. Second, magnetometer systems do not record other behavioral effects of the drugs outside of the HTR. Our validation testing suggests that our approach may detect the HTR more accurately than visual scoring in some cases, as some false positive HTR events were actually true positives missed by multiple trained visual raters. Another benefit of our approach compared to automated

magnetometer-based methods is expanding detection to include additional behaviors. Indeed, SimBA is designed for classification of multiple user-defined, complex animal behaviors.[35] Previous studies have successfully deployed DLC+SimBA to examine social behaviors in both rats and mice.[76, 77] Existing approaches are limited in detection of additional behaviors, while our approach allows investigators to interrogate experimental recordings for novel behavioral insights, which is especially relevant given the developing chemical landscape of psychedelic drugs. It is well-established that indoleamine psychedelics are nonselective receptor agonists, and produce complex behavioral effects in rodents outside of the HTR that may warrant further investigation.[32, 34, 59, 78-80] Our approach uniquely provides the modularity to quantify and evaluate other behaviors of potential interest, by training new SimBA classifiers on top of already produced DLC annotations. Overall, the observations support the utility of experimental video recordings in HTR detection set ups.

Despite some limitations of the magnetometer-based detection approaches, the counts are reported to be highly accurate, the data acquisition can be rapid with automated ML-based approaches, and these systems are better equipped to study the dynamics of the head movements during individual HTR events.[1, 5, 13, 15, 16] Magnetometer systems can distinguish between subtypes of HTR events (e.g. short vs. long or low vs. high amplitude).[16] The present automated DLC+SimBA approach is limited in this regard, but it is possible that future iterations, perhaps with higher frame rate videos, may be able to accurately track the speed and dynamics of head movements during HTR events.

Data acquisition for the present DLC+SimBA approach is also slower compared to automated magnetometer-based approaches. Using the methods and equipment described here, however, it is possible to acquire data by the following morning, if DLC analysis commences at the end of a workday. Moreover, the present approach is flexible and scalable beyond the specific methods described here. While analyzing new videos with a DLC pose estimation model is computationally expensive, using DLC with cloud-based computing resource services can allow investigators to train and deploy a pose estimation model for free or low cost, then run SimBA on a local computer. Furthermore, using cloud-based computing resources, an institution's high-performance computing cluster, or multiple graphical processing units (GPU), investigators can analyze experimental videos in parallel, significantly reducing data acquisition time to provide same-day results if desired. Future experiments should examine real-time pose estimation or other ML-based behavioral quantification approaches, such as with DLC-Live!, to further reduce data acquisition time.[81] Our approach lays the foundation for others to improve and expand these methods for even more rapid HTR detection and data acquisition.

The present validation studies also demonstrate that accurate detection of HTR can be achieved even with lower to moderate resolution and frame rate videos (50% resolution, 60 fps), suggesting that investigators can potentially use inexpensive video recording equipment. Furthermore, excellent HTR detection performance was achieved using only 30 historical experimental videos to train DLC pose estimation models and 10 videos featuring 136 HTR events to train SimBA behavioral classifiers. The small amount of training data required for models with good performance highlights the accessibility of setting up the present approach. Additionally, both the DLC and Simple Behavioral Analysis toolkits are open-source with extensive documentation and software updates [24, 35], and have been employed in diverse behavioral neuroscience paradigms.[76, 77] Investigators should leverage the insights from our approach to guide the training, validation, and deployment of a DLC+SimBA model combination to detect HTR that is optimized for each laboratory.

To aid with deployment of this approach in other laboratories, here are several recommendations for investigators to implement and streamline this process. First, as with the implementation of any novel assay, investigators should implement reasonable controls, such as manually reviewing a small segment of experimental video to compare with visual HTR counts. Additionally, including a single dose positive control compound such as DOI (1 mg/kg) will allow comparison of counts across laboratories and scoring approaches. Second, while training a model and analyzing new videos with a DLC pose estimation model is computationally expensive and requires a mid-range GPU, using DLC with cloud-based computing resource services, such as Google Colab or Amazon Web Services, could bypass this problem. Investigators can easily train and deploy a pose estimation model for free or low cost, then run SimBA on their local computer. Third, to further enable "plug-and-play" of this approach, investigators may also consider implementing generalizable DLC models pre-trained to predict key points across animals (e.g. SuperAnimal models from the Mathis lab), which can readily track mice and be fine-tuned by investigators to accommodate variable experimental setups, further reducing the burden of annotating body parts for a new pose estimation model.[82]

Conclusions

Our results show that using DLC+SimBA is a rapid, accurate, open-source, automated, and non-invasive approach for the assessment of HTRs in mice. This approach requires minimal training data and equipment, yet demonstrates excellent performance rivaling existing automated methods. Behavioral control experiments, robust validation testing, and post-hoc explainability metrics further support feasibility and reliability of the approach. To further assess the utility of this approach in psychedelic drug discovery, the HTR potency and efficacy of bufotenine was studied, revealing that 5-HT_{1A}-mediated effects of the drug attenuate its effects on HTR in mice. Furthermore, the potent selective SERT release properties of bufotenine may be relevant to its overall pharmacological effects. In summary,

the present findings support the deployment of the DLC+SimBA HTR detection approach in mice and demonstrate key advantages over existing methods.

Methods

3.1 Workflow overview and experimental design

For training and assessing our DLC and SimBA model combinations, 78 historical experimental videos were selected, primarily ranging from 12 to 17 minutes in length. Videos were randomly selected across animals, drug doses, session timepoints, cylinder alignments, lighting conditions, and experiment days to maximize training and testing set diversity for robust DLC and SimBA models. To avoid training-testing leakage, a common pitfall of ML-based approaches [83], videos were randomly segregated into non-overlapping training and validation sets. For the final models, 30 videos were used for training the body part tracker using DLC (DLC training subset), 10 videos for training the behavioral classifier using SimBA (SimBA training subset), and 38 hold-out videos to assess the performance of the final DLC+SimBA model combinations for HTR detection by calculating the precision, recall, and F_1 scores (training subset; **Figure 1B**). The validation subset videos included 18 experimental videos from Glatfelter et al. [19], and 20 additional random historical experimental videos across various psychedelic drugs (i.e. psilocybin, LSD, DOI, DOBU, 2,5-DMA, DOPR), doses (0.001 – 30 mg/kg), lighting conditions (standard room overhead and enhanced lighting), and animals (male and female), for a total of 38 experimental videos (**Figure 1B**). Each of the 9 behavioral classifiers were assessed at various discrimination thresholds, from 0% to 50%.

Briefly, all drug experimental videos used the following parameters, as described in detail by Glatfelter et al. [19]. Hero Black 7 GoPro cameras (GoPro Inc.) were used to record 120 fps videos at 1280 x 960 resolution. For the experimental sessions, mice received drug or vehicle injections and were placed into cylindrical acrylic arenas (7.5 in diameter) housed inside of TruScan mouse locomotor boxes (Coulbourn Instruments). The arenas had transparent floor panels with white bench paper underneath to provide a light background for contrast. GoPro cameras were mounted ~ 10 inches above the arena floor, and experimental test sessions were recorded for 30 min post injection. All experiments occurred during the light phase of the light–dark cycle between 0800 and 1700 h local time. Subjects were randomized to treatment conditions and were repeat tested once per 1–2 weeks to avoid tolerance to the effects of each drug on HTR. After videos of each experiment were recorded, the video files were transferred to an external hard drive for storage until subsequent training and analysis as described below.

3.2 Video pre-processing

To assess combined DLC+SimBA model performances across video resolutions and frame rates, all 78 videos were batch preprocessed using FFmpeg, a free, open-source software tool

for handling video files (https://www.ffmpeg.org/). The video files were downscaled from 1280 x 960 pixels (100% resolution), 120 fps to 906 x 680 pixels (50% resolution), 640 x 480 pixels (25% resolution), and 454 x 340 pixels (12.5% resolution) at 120, 60, and 30 fps. In summary, for training and assessing the DLC and SimBA models, there were 9 sets of 78 videos, representing each resolution and frame rate.

3.3 Mouse pose estimation models

For body part tracking, DLC (version 2.3) [(Mathis et al. 2018), (Nath et al. 2019)] was used for training a model at each video resolution (50%, 25%, 12.5%). Specifically, extracted frames taken from 30 videos (at each resolution) and 16 animals (then 95% was used for training) were labeled. The number of total extracted frames was 600 frames for each DLC model. Thirteen body points were consistently labeled, including nose, left eye, right eye, left ear, right ear, top of the skull, three points along the spine, the tail base, and three points along the tail (**Figure 1A**). A ResNet-50-based neural network [84, 85] was used with default parameters (batch size of 8) for 500,000 training iterations, when loss typically plateaus.[23] Each model was validated with 3 shuffles. The train and test errors for each model can be found in **Table S1**, as well as comparisons of each models' analysis times in **Table S2**. Prior to behavioral classifier training using SimBA, two internal controls videos of an empty cylinder arena and a historical experimental video featuring an immobile mouse were analyzed to further validate each DLC model.

3.4 Behavioral classifiers

Behavioral classifiers were generated with 13 user-defined body parts in SimBA for each video resolution and frame rate, for a total of 9 behavioral classifiers. Since the same set of historical experimental videos were used, the HTR event annotations were copied across resolutions. For example, the behavioral classifier trained at 50% resolution, 30 fps had identical behavior annotations as the behavioral classifier trained at 25% resolution, 30 fps. The approximate width of the TruScan chamber was used to define pixels per mm during the Video Settings step. The outlier correction step was skipped. Features derived from mouse pose estimation data (32 features) were extracted using default settings.

Classifier training videos were carefully annotated for the HTR using the default SimBA behavioral annotator GUI. A total of 1,212,960 frames (at 120 fps), 606,480 frames (at 60 fps), and 303,240 frames (at 30 fps) from 10 random historical experimental videos at each resolution (2.8 h of video recording) were annotated for HTR events. Each HTR was annotated from the initial movement of the mouse's ears until the head returned to its initial resting state. Frequencies of annotated HTR behavior in the training subset were 0.13% at 30 fps, 0.1% at 60 fps, and 0.09% at 120 fps. To further confirm model performance was not dependent on a specific labeler, the same classifier training videos were also carefully

annotated for HTR by another experimenter using methods described above. Random forest models were generated in SimBA with the default hyperparameters.

3.5 Post-hoc explainability metrics for behavioral classifiers

Feature importance values were calculated for each behavioral classifier in SimBA. SHAP analyses were run on 100 random frames with HTR behavior present and 100 random frames with HTR behavior absent for each model. Feature importance values are provided in **Figure 4**. SHAP value correlations can be provided upon reasonable request.

3.6 Behavioral control experimental videos

Previously recorded experimental videos of d-amphetamine-induced locomotion and stereotypy and SKF-38393-induced grooming from Glatfelter et al. [19] were analyzed using the best performing DLC and SimBA model combination. For detailed methods for drug-induced behavioral control experiments, see Glatfelter et al. [19].

3.7 Bufotenine dose-response experiments

Prior to each experiment, mouse body weight and temperature were recorded. Mice were then placed into testing chambers for acclimation. In dose–response studies, after a brief 5 min acclimation, mouse body temperature was recorded for baseline measurement, mice received a s.c. injection of bufotenine or vehicle, and animals were returned to the testing arena for 30 min. During the session, locomotor activity was monitored via photobeam tracking of movements in the horizontal plane to yield distance traveled in centimeters. Video recordings used GoPro Hero Black 7 cameras (1280 x 960, 120 fps). Post-treatment body temperature values were also recorded. In antagonist reversal experiments, mice received a s.c. injection of either WAY100635 or vehicle 10 mins prior to bufotenine and were returned to the testing chamber for 30 mins. During this period, locomotor activity was monitored to examine the potential effects of antagonist treatment on general behavior or movement.

3.8 Computer hardware and software for machine learning models

All models were trained on a Dell Precision Workstation T5820 with Intel Xeon Processor W-2223 (3.6GHz), 32 GB RAM, Windows 11 Pro operating system, and a NVIDIA RTX A4000 GPU (video card). Videos were downscaled using FFmpeg. Pose estimation models were trained using DLC version 2.3.10. Behavioral classifiers were generated using SimBA version 2.2.4.

3.9 Data Analysis and Statistics

Data for the acute effects of bufotenine on HTR were fit with biphasic dose-response nonlinear regression fits for visualization. Data for acute effects of bufotenine on body temperature change and motor activity were fit with four parameter nonlinear regression

fits (IC_{50} > 0) except the motor activity for WAY pretreatment. Potency values for HTR were determined using four parameter nonlinear regression fits of ascending limb doses of bufotenine+WAY (EC_{50} > 0). Comparisons of dose-response data for acute drug effects (HTR, body temperature change, motor activity) were conducted via two-way ANOVA (dose x treatment) with Sidak's post hoc tests. Predetermined comparisons were made within treatment (no pretreatment and WAY pretreatment) vs. respective 0 dose controls and between treatments dose by dose. Pearson correlation analyses (two tailed) were conducted to assess relationships between HTR counts across scoring methods. Alpha was set at 0.05 for all analyses. Three parameter nonlinear regression fits were used to determine best fit values of interest (IC_{50}, EC_{50}, E_{max}) in monoamine transporter assays.

3.10 In Vitro Transporter Assays

Transporter experiments were conducted as previously described.[48, 86-88] Briefly, Sprague-Dawley rats were euthanized via CO_2 narcosis and brain tissue collected. Specifically, tissue from the caudate was used for dopamine transporter assays, while caudate and cerebellum tissue were used for the norepinephrine transporter and SERT assays. Using differential centrifugation, synaptosomal fractions were obtained from the tissue. Synaptosomal preparations were utilized for both uptake and release assays with tritiated neurotransmitters (5-HT, dopamine, norepinephrine).

Author Contributions

Experimental design - A.D.M, G.C.G., M.H.B.
Scoring and validation – A.D.M, D.W., N.R.G., G.C.G.
Mouse experiments – G.C.G., A.D.M., N.R.G.
Data analyses – G.C.G., A.D.M., F. P.
Editing and proofreading – G.C.G., M.H.B., F.P.

Abbreviations

DeepLabCut = DLC
DOI = 2,5-dimethoxy-4-iodoamphetamine
DOBU = 2,5-dimethoxy-4-butylamphetamine
DOPR = 2,5-dimethoxy-4-propylamphetamine
2,5-DMA = 2,5-dimethoxyamphetamine
LSD = lysergic acid diethylamide
Fps = frames per second
Head-twitch response = HTR
Machine learning = ML
Simple Behavioral Analysis = SimBA
Serotonin = 5-HT
Serotonin 1A receptors = $5\text{-}HT_{1A}$

Serotonin 2A receptor = 5-HT_{2A}
Serotonin transporter = SERT
5-HO-DMT = 5-hydroxy-*N*,*N*-dimethyltryptamine
5-MeO-DMT = 5-methoxy-*N*,*N*-dimethyltryptamine
DMT = *N*,*N*-dimethyltryptamine
WAY = WAY100635

Supporting Information

Final snapshot table for the DLC model at each video resolution; DLC inference time and FFmpeg downscaling time cost table; heatmap plots of accuracy-discrimination threshold curve summary data; accuracy-discrimination threshold curves from a second experimenter; heatmap plots of accuracy-discrimination threshold curve summary data from a second experimenter; time-course plots for acute effects of bufotenine on the HTR; time-course plots for acute effects of bufotenine on motor activity; summary statistics table for acute effects of bufotenine; heatmap plots illustrating monoamine transporter activity of bufotenine.

Author Information

Corresponding Author

Grant C. Glatfelter - Designer Drug Research Unit, Intramural Research Program, National Institute on Drug Abuse, Baltimore, Maryland 21224, United States; Email: grant.glatfelter@nih.gov

Authors

Alexander D. Maitland - Designer Drug Research Unit, Intramural Research Program, National Institute on Drug Abuse, Baltimore, Maryland 21224, United States

Nicholas R. Gonzalez - Designer Drug Research Unit, Intramural Research Program, National Institute on Drug Abuse, Baltimore, Maryland 21224, United States

Donna Walther - Designer Drug Research Unit, Intramural Research Program, National Institute on Drug Abuse, Baltimore, Maryland 21224, United States

Francisco Pereira - Machine Learning Core, National Institute of Mental Health, National Institutes of Health, Bethesda, Maryland 20814, United States

Michael H. Baumann - Designer Drug Research Unit, Intramural Research Program, National Institute on Drug Abuse, Baltimore, Maryland 21224, United States

Acknowledgements

This work was supported by NIDA Intramural Research Program grant number DA-000522-16 (M.H.B.). We would like to thank the Mathis Laboratory and Golden Laboratory for their open-source toolkits, DLC and Simple Behavioral Analysis respectively. We would like to especially thank Simon Nilsson of the Golden Laboratory for their insights on the community

Github forums. The structure in **Figure 6A** and the graphical abstract were created using ChemDraw (v 21.0.0).

References

(1) Halberstadt, A. L., and Geyer, M. A. (**2013**) Characterization of the head-twitch response induced by hallucinogens in mice: detection of the behavior based on the dynamics of head movement, *Psychopharmacology (Berl) 227*, 727-739, DOI: 10.1007/s00213-013-3006-z.
(2) González-Maeso, J., Weisstaub, N. V., Zhou, M., Chan, P., Ivic, L., Ang, R., Lira, A., Bradley-Moore, M., Ge, Y., Zhou, Q., Sealfon, S. C., and Gingrich, J. A. (**2007**) Hallucinogens Recruit Specific Cortical 5-HT2A Receptor-Mediated Signaling Pathways to Affect Behavior, *Neuron 53*, 439-452, DOI: https://doi.org/10.1016/j.neuron.2007.01.008.
(3) Canal, C. E., and Morgan, D. (**2012**) Head-twitch response in rodents induced by the hallucinogen 2,5-dimethoxy-4-iodoamphetamine: a comprehensive history, a re-evaluation of mechanisms, and its utility as a model, *Drug Test Anal 4*, 556-576, DOI: 10.1002/dta.1333.
(4) Nichols, D. E. (**2016**) Psychedelics, *Pharmacological Reviews 68*, 264-355, DOI: 10.1124/pr.115.011478.
(5) Halberstadt, A. L., Chatha, M., Klein, A. K., Wallach, J., and Brandt, S. D. (**2020**) Correlation between the potency of hallucinogens in the mouse head-twitch response assay and their behavioral and subjective effects in other species, *Neuropharmacology 167*, 107933, DOI: https://doi.org/10.1016/j.neuropharm.2019.107933.
(6) Fantegrossi, W. E., Simoneau, J., Cohen, M. S., Zimmerman, S. M., Henson, C. M., Rice, K. C., and Woods, J. H. (**2010**) Interaction of 5-HT2A and 5-HT2C receptors in R(-)-2,5-dimethoxy-4-iodoamphetamine-elicited head twitch behavior in mice, *J Pharmacol Exp Ther 335*, 728-734, DOI: 10.1124/jpet.110.172247.
(7) Cameron, L. P., Tombari, R. J., Lu, J., Pell, A. J., Hurley, Z. Q., Ehinger, Y., Vargas, M. V., McCarroll, M. N., Taylor, J. C., Myers-Turnbull, D., Liu, T., Yaghoobi, B., Laskowski, L. J., Anderson, E. I., Zhang, G., Viswanathan, J., Brown, B. M., Tjia, M., Dunlap, L. E., Rabow, Z. T., Fiehn, O., Wulff, H., McCorvy, J. D., Lein, P. J., Kokel, D., Ron, D., Peters, J., Zuo, Y., and Olson, D. E. (**2021**) A non-hallucinogenic psychedelic analogue with therapeutic potential, *Nature 589*, 474-479, DOI: 10.1038/s41586-020-3008-z.
(8) Darmani, N. A., Shaddy, J., and Gerdes, C. F. (**1996**) Differential Ontogenesis of Three DOI-Induced Behaviors in Mice, *Physiology & Behavior 60*, 1495-1500, DOI: https://doi.org/10.1016/S0031-9384(96)00323-X.
(9) Erkizia-Santamaría, I., Alles-Pascual, R., Horrillo, I., Meana, J. J., and Ortega, J. E. (**2022**) Serotonin 5-HT2A, 5-HT2c and 5-HT1A receptor involvement in the acute effects of psilocybin in mice. In vitro pharmacological profile and modulation of thermoregulation and head-twich response, *Biomedicine & Pharmacotherapy 154*, 113612, DOI: https://doi.org/10.1016/j.biopha.2022.113612.
(10) Canal, C. E., Olaghere da Silva, U. B., Gresch, P. J., Watt, E. E., Sanders-Bush, E., and Airey, D. C. (**2010**) The serotonin 2C receptor potently modulates the head-twitch response in mice induced by a phenethylamine hallucinogen, *Psychopharmacology (Berl) 209*, 163-174, DOI: 10.1007/s00213-010-1784-0.
(11) Holloway, T., Moreno, J. L., and González-Maeso, J. (**2016**) HSV-Mediated Transgene Expression of Chimeric Constructs to Study Behavioral Function of GPCR Heteromers in Mice. *Journal of visualized experiments : JoVE* DOI: 10.3791/53717.
(12) U.S. Department of Health and Human Services: Office of Disease Prevention and Health Promotion--Healthy People 2020, *Nasnewsletter 15*, 3.
(13) de la Fuente Revenga, M., Shin, J. M., Vohra, H. Z., Hideshima, K. S., Schneck, M., Poklis, J. L., and González-Maeso, J. (**2019**) Fully automated head-twitch detection system for the

study of 5-HT(2A) receptor pharmacology in vivo, *Sci Rep 9*, 14247, DOI: 10.1038/s41598-019-49913-4.
(14) Jaster, A. M., and González-Maeso, J. (**2023**) Automated Detection of Psychedelic-Induced Head-Twitch Response in Mice. In *Schizophrenia: Methods and Protocols* (Urigüen, L., and Díez-Alarcia, R., Eds.), pp 65-76, Springer US, New York, NY.
(15) de la Fuente Revenga, M., Vohra, H. Z., and González-Maeso, J. (**2020**) Automated quantification of head-twitch response in mice via ear tag reporter coupled with biphasic detection, *Journal of Neuroscience Methods 334*, 108595, DOI: https://doi.org/10.1016/j.jneumeth.2020.108595.
(16) Halberstadt, A. L. (**2020**) Automated detection of the head-twitch response using wavelet scalograms and a deep convolutional neural network, *Scientific reports 10*, 8344-8344, DOI: 10.1038/s41598-020-65264-x.
(17) Siegel, R. K., Lee, M. A., and Jarvik, M. E. (**1972**) A device for analyzing drug-induced responses in freely moving mice, *Journal of the experimental analysis of behavior 18*, 415-418, DOI: 10.1901/jeab.1972.18-415.
(18) Nakamura, M., Hojo, M., Kawai, A., Ikushima, K., Nagasawa, A., Takahashi, H., Makino, K., Suzuki, T., Suzuki, J., and Inomata, A. (**2023**) An application of the magnetometer detection system to Crl:CD1 (ICR) mice for head twitch response induced by hallucinogenic 5-HT_{2A} agonists, *Fundamental Toxicological Sciences 10*, 189-197, DOI: 10.2131/fts.10.189.
(19) Glatfelter, G. C., Chojnacki, M. R., McGriff, S. A., Wang, T., and Baumann, M. H. (**2022**) Automated Computer Software Assessment of 5-Hydroxytryptamine 2A Receptor-Mediated Head Twitch Responses from Video Recordings of Mice, *ACS Pharmacology & Translational Science*, DOI: 10.1021/acsptsci.1c00237.
(20) Sturman, O., von Ziegler, L., Schläppi, C., Akyol, F., Privitera, M., Slominski, D., Grimm, C., Thieren, L., Zerbi, V., Grewe, B., and Bohacek, J. (**2020**) Deep learning-based behavioral analysis reaches human accuracy and is capable of outperforming commercial solutions, *Neuropsychopharmacology 45*, 1942-1952, DOI: 10.1038/s41386-020-0776-y.
(21) Contreras, A., Khumnark, M., Hines, R. M., and Hines, D. J. (**2021**) Behavioral arrest and a characteristic slow waveform are hallmark responses to selective 5-HT2A receptor activation, *Scientific Reports 11*, 1925, DOI: 10.1038/s41598-021-81552-6.
(22) Cyrano, E., and Popik, P. (**2025**) Assessing the effects of 5-HT2A and 5-HT5A receptor antagonists on DOI-induced head-twitch response in male rats using marker-less deep learning algorithms, *Pharmacological Reports 77*, 135-144, DOI: 10.1007/s43440-024-00679-1.
(23) Mathis, A., Mamidanna, P., Cury, K. M., Abe, T., Murthy, V. N., Mathis, M. W., and Bethge, M. (**2018**) DeepLabCut: markerless pose estimation of user-defined body parts with deep learning, *Nature Neuroscience 21*, 1281-1289, DOI: 10.1038/s41593-018-0209-y.
(24) Nath, T., Mathis, A., Chen, A. C., Patel, A., Bethge, M., and Mathis, M. W. (**2019**) Using DeepLabCut for 3D markerless pose estimation across species and behaviors, *Nature Protocols 14*, 2152-2176, DOI: 10.1038/s41596-019-0176-0.
(25) Shulgin, A. T., and Shulgin, A. (**1997**) *TiHKAL: The Continuation*, Transform Press.
(26) Ott, J. (**2001**) Pharmañopo—Psychonautics: Human Intranasal, Sublingual, Intrarectal, Pulmonary and Oral Pharmacology of Bufotenine, *Journal of Psychoactive Drugs 33*, 273-281, DOI: 10.1080/02791072.2001.10400574.
(27) Fabing, H. D., and Hawkins, J. R. (**1956**) Intravenous Bufotenine Injection in the Human Being, *Science 123*, 886-887, DOI: doi:10.1126/science.123.3203.886.
(28) McLeod, W. R., and Sitaram, B. R. (**1985**) Bufotenine reconsidered, *Acta Psychiatrica Scandinavica 72*, 447-450, DOI: https://doi.org/10.1111/j.1600-0447.1985.tb02638.x.
(29) McBride, M. C. (**2000**) Bufotenine: Toward an Understanding of Possible Psychoactive Mechanisms, *Journal of Psychoactive Drugs 32*, 321-331, DOI: 10.1080/02791072.2000.10400456.

(30) Sherwood, A. M., Burkhartzmeyer, E. K., Williamson, S. E., Baumann, M. H., and Glatfelter, G. C. (**2024**) Psychedelic-like Activity of Norpsilocin Analogues, *ACS Chemical Neuroscience 15*, 315-327, DOI: 10.1021/acschemneuro.3c00610.
(31) Glatfelter, G. C., Pottie, E., Partilla, J. S., Stove, C. P., and Baumann, M. H. (**2024**) Comparative Pharmacological Effects of Lisuride and Lysergic Acid Diethylamide Revisited, *ACS Pharmacology & Translational Science*.
(32) Glatfelter, G. C., Clark, A. A., Cavalco, N. G., Landavazo, A., Partilla, J. S., Naeem, M., Golen, J. A., Chadeayne, A. R., Manke, D. R., Blough, B. E., McCorvy, J. D., and Baumann, M. H. (**2024**) Serotonin 1A Receptors Modulate Serotonin 2A Receptor-Mediated Behavioral Effects of 5-Methoxy-N,N-dimethyltryptamine Analogs in Mice, *ACS Chemical Neuroscience*, DOI: 10.1021/acschemneuro.4c00513.
(33) Glatfelter, G. C., Naeem, M., Pham, D. N. K., Golen, J. A., Chadeayne, A. R., Manke, D. R., and Baumann, M. H. (**2023**) Receptor Binding Profiles for Tryptamine Psychedelics and Effects of 4-Propionoxy-N,N-dimethyltryptamine in Mice, *ACS Pharmacology & Translational Science*, DOI: 10.1021/acsptsci.2c00222.
(34) Glatfelter, G. C., Pottie, E., Partilla, J. S., Sherwood, A. M., Kaylo, K., Pham, D. N. K., Naeem, M., Sammeta, V. R., DeBoer, S., Golen, J. A., Hulley, E. B., Stove, C. P., Chadeayne, A. R., Manke, D. R., and Baumann, M. H. (**2022**) Structure-Activity Relationships for Psilocybin, Baeocystin, Aeruginascin, and Related Analogues to Produce Pharmacological Effects in Mice, *ACS Pharmacol Transl Sci 5*, 1181-1196, DOI: 10.1021/acsptsci.2c00177.
(35) Goodwin, N. L., Choong, J. J., Hwang, S., Pitts, K., Bloom, L., Islam, A., Zhang, Y. Y., Szelenyi, E. R., Tong, X., Newman, E. L., Miczek, K., Wright, H. R., McLaughlin, R. J., Norville, Z. C., Eshel, N., Heshmati, M., Nilsson, S. R. O., and Golden, S. A. (**2024**) Simple Behavioral Analysis (SimBA) as a platform for explainable machine learning in behavioral neuroscience, *Nature Neuroscience 27*, 1411-1424, DOI: 10.1038/s41593-024-01649-9.
(36) Breiman, L., Friedman, J., Olshen, R. A., and Stone, C. J. (**1984**) *Classification and Regression Trees*, 1st ed., Chapman and Hall/CRC DOI: https://doi.org/10.1201/9781315139470.
(37) Zhang, M., Yang, Y., Yang, Z., Wen, X., Zhang, C., Xiao, P., Wang, Y., Sun, J., Wang, H., and Wang, X. (**2025**) Structural insights into tryptamine psychedelics: The role of hydroxyl indole ring site in 5-HT2A receptor activation and psychedelic-like activity, *European Journal of Medicinal Chemistry 281*, 117049, DOI: https://doi.org/10.1016/j.ejmech.2024.117049.
(38) Puigseslloses, P., Nadal-Gratacós, N., Ketsela, G., Weiss, N., Berzosa, X., Estrada-Tejedor, R., Islam, M. N., Holy, M., Niello, M., Pubill, D., Camarasa, J., Escubedo, E., Sitte, H. H., and López-Arnau, R. (**2024**) Structure-activity relationships of serotonergic 5-MeO-DMT derivatives: insights into psychoactive and thermoregulatory properties, *Molecular Psychiatry*, DOI: 10.1038/s41380-024-02506-8.
(39) Lyttle, T., David, G., and and Gartz, J. (**1996**) Bufo Toads and Bufotenine: Fact and Fiction Surrounding an Alleged Psychedelic, *Journal of Psychoactive Drugs 28*, 267-290, DOI: 10.1080/02791072.1996.10472488.
(40) Shulgin, A. T. (**1981**) Bufotenine, *Journal of Psychoactive Drugs 13*, 389-389, DOI: 10.1080/02791072.1981.10471899.
(41) TURNER, W. J., and MERLIS, S. (**1959**) Effect of Some Indolealkylamines on Man, *A.M.A. Archives of Neurology & Psychiatry 81*, 121-129, DOI: 10.1001/archneurpsyc.1959.02340130141020.
(42) Chilton, W. S., Jeremy, B., and and Jensen, R. E. (**1979**) Psilocin, Bufotenine and Serotonin: Historical and Biosynthetic Observations, *Journal of Psychedelic Drugs 11*, 61-69, DOI: 10.1080/02791072.1979.10472093.
(43) Delices, M., Muller, J. d. A. I., Arunachalam, K., and Martins, D. T. d. O. (**2023**) Anadenanthera colubrina (Vell) Brenan: Ethnobotanical, phytochemical, pharmacological and

toxicological aspects, *Journal of Ethnopharmacology 300*, 115745, DOI: https://doi.org/10.1016/j.jep.2022.115745.
(44) Moretti, C., Gaillard, Y., Grenand, P., Bévalot, F., and Prévosto, J.-M. (**2006**) Identification of 5-hydroxy-tryptamine (bufotenine) in takini (Brosimum acutifolium Huber subsp. acutifolium C.C. Berg, Moraceae), a shamanic potion used in the Guiana Plateau, *Journal of Ethnopharmacology 106*, 198-202, DOI: https://doi.org/10.1016/j.jep.2005.12.022.
(45) Barry, T. L., Petzinger, G., and Zito, S. W. (**1996**) GC/MS comparison of the West Indian aphrodisiac "Love Stone" to the Chinese medication "chan su": bufotenine and related bufadienolides, *J Forensic Sci 41*, 1068-1073.
(46) Chamakura, R. P. (**1994**) Bufotenine - A Hallucinogen in Ancient Snuff Powders of South America and a Drug of Abuse on the Streets of New York City, *Forensic Sci Rev 6*, 1-18.
(47) Barker, S. A., McIlhenny, E. H., and Strassman, R. (**2012**) A critical review of reports of endogenous psychedelic N, N-dimethyltryptamines in humans: 1955–2010, *Drug Testing and Analysis 4*, 617-635, DOI: https://doi.org/10.1002/dta.422.
(48) Blough, B. E., Landavazo, A., Decker, A. M., Partilla, J. S., Baumann, M. H., and Rothman, R. B. (**2014**) Interaction of psychoactive tryptamines with biogenic amine transporters and serotonin receptor subtypes, *Psychopharmacology 231*, 4135-4144, DOI: 10.1007/s00213-014-3557-7.
(49) Roth, B. L., Choudhary, M. S., Khan, N., and Uluer, A. Z. (**1997**) High-affinity agonist binding is not sufficient for agonist efficacy at 5-hydroxytryptamine2A receptors: evidence in favor of a modified ternary complex model, *J Pharmacol Exp Ther 280*, 576-583.
(50) Choudhary, M. S., Craigo, S., and Roth, B. L. (**1993**) A single point mutation (Phe340-->Leu340) of a conserved phenylalanine abolishes 4-[125I]iodo-(2,5-dimethoxy)phenylisopropylamine and [3H]mesulergine but not [3H]ketanserin binding to 5-hydroxytryptamine2 receptors, *Mol Pharmacol 43*, 755-761.
(51) Pauwels, P. J., Van Gompel, P., and Leysen, J. E. (**1993**) Activity of serotonin (5-HT) receptor agonists, partial agonists and antagonists at cloned human 5-HT1a receptors that are negatively coupled to adenylate cyclase in permanently transfected hela cells, *Biochemical Pharmacology 45*, 375-383, DOI: https://doi.org/10.1016/0006-2952(93)90073-6.
(52) Williams, G. M., Smith, D. L., and Smith, D. J. (**1992**) 5-HT3 receptors are not involved in the modulation of the K+-evoked release of [3H]5-HT from spinal cord synaptosomes of rat, *Neuropharmacology 31*, 725-733, DOI: https://doi.org/10.1016/0028-3908(92)90033-L.
(53) Peroutka, S. J. (**1985**) Selective labeling of 5-HT1A and 5-HT1B binding sites in bovine brain, *Brain Research 344*, 167-171, DOI: https://doi.org/10.1016/0006-8993(85)91204-1.
(54) Kozell, L. B., Eshleman, A. J., Swanson, T. L., Bloom, S. H., Wolfrum, K. M., Schmachtenberg, J. L., Olson, R. J., Janowsky, A. J., and Abbas, A. I. (**2023**) Pharmacologic activity of substituted tryptamines at 5-HT(2A)R, 5-HT(2C)R, 5-HT(1A)R, and SERT, *J Pharmacol Exp Ther*, DOI: 10.1124/jpet.122.001454.
(55) Cozzi, N. V., Gopalakrishnan, A., Anderson, L. L., Feih, J. T., Shulgin, A. T., Daley, P. F., and Ruoho, A. E. (**2009**) Dimethyltryptamine and other hallucinogenic tryptamines exhibit substrate behavior at the serotonin uptake transporter and the vesicle monoamine transporter, *Journal of Neural Transmission 116*, 1591-1599, DOI: 10.1007/s00702-009-0308-8.
(56) Becker, A. M., Klaiber, A., Holze, F., Istampoulouoglou, I., Duthaler, U., Varghese, N., Eckert, A., and Liechti, M. E. (**2023**) Ketanserin Reverses the Acute Response to LSD in a Randomized, Double-Blind, Placebo-Controlled, Crossover Study in Healthy Participants, *Int J Neuropsychopharmacol 26*, 97-106, DOI: 10.1093/ijnp/pyac075.
(57) Preller, K. H., Herdener, M., Pokorny, T., Planzer, A., Kraehenmann, R., Stämpfli, P., Liechti, M. E., Seifritz, E., and Vollenweider, F. X. (**2017**) The Fabric of Meaning and Subjective Effects in LSD-Induced States Depend on Serotonin 2A Receptor Activation, *Curr Biol 27*, 451-457, DOI: 10.1016/j.cub.2016.12.030.

(58) Vollenweider, F. X., Vollenweider-Scherpenhuyzen, M. F., Bäbler, A., Vogel, H., and Hell, D. (**1998**) Psilocybin induces schizophrenia-like psychosis in humans via a serotonin-2 agonist action, *Neuroreport 9*, 3897-3902, DOI: 10.1097/00001756-199812010-00024.
(59) Brandt, S. D., Kavanagh, P. V., Twamley, B., Westphal, F., Elliott, S. P., Wallach, J., Stratford, A., Klein, L. M., McCorvy, J. D., Nichols, D. E., and Halberstadt, A. L. (**2018**) Return of the lysergamides. Part IV: Analytical and pharmacological characterization of lysergic acid morpholide (LSM-775), *Drug Test Anal 10*, 310-322, DOI: 10.1002/dta.2222.
(60) Warren, A. L., Lankri, D., Cunningham, M. J., Serrano, I. C., Parise, L. F., Kruegel, A. C., Duggan, P., Zilberg, G., Capper, M. J., Havel, V., Russo, S. J., Sames, D., and Wacker, D. (**2024**) Structural pharmacology and therapeutic potential of 5-methoxytryptamines, *Nature*, DOI: 10.1038/s41586-024-07403-2.
(61) Pokorny, T., Preller, K. H., Kraehenmann, R., and Vollenweider, F. X. (**2016**) Modulatory effect of the 5-HT1A agonist buspirone and the mixed non-hallucinogenic 5-HT1A/2A agonist ergotamine on psilocybin-induced psychedelic experience, *Eur Neuropsychopharmacol 26*, 756-766, DOI: 10.1016/j.euroneuro.2016.01.005.
(62) Gattuso, J. J., Wilson, C., Li, S., Hannan, A. J., and Renoir, T. (**2025**) Mice lacking the serotonin transporter do not respond to the behavioural effects of psilocybin, *European Journal of Pharmacology 991*, 177304, DOI: https://doi.org/10.1016/j.ejphar.2025.177304.
(63) Becker, A. M., Humbert-Droz, M., Mueller, L., Jelusic, A., Tolev, A., Straumann, I., Avedisian, I., Erne, L., Thomann, J., Luethi, D., Grunblatt, E., Meyer Zu Schwabedissen, H., and Liechti, M. E. (**2025**) Acute Effects and Pharmacokinetics of LSD after Paroxetine or Placebo Pre-Administration in a Randomized, Double-Blind, Cross-Over Phase I Trial, *Clin Pharmacol Ther n/a*, DOI: 10.1002/cpt.3618.
(64) Krall, C. M., Richards, J. B., Rabin, R. A., and Winter, J. C. (**2008**) Marked decrease of LSD-induced stimulus control in serotonin transporter knockout mice, *Pharmacology Biochemistry and Behavior 88*, 349-357, DOI: https://doi.org/10.1016/j.pbb.2007.09.006.
(65) Qu, Y., Villacreses, N., Murphy, D. L., and Rapoport, S. I. (**2005**) 5-HT2A/2C receptor signaling via phospholipase A2 and arachidonic acid is attenuated in mice lacking the serotonin reuptake transporter, *Psychopharmacology 180*, 12-20, DOI: 10.1007/s00213-005-2231-5.
(66) Glatfelter, G., Walther, D., Partilla, J., Chadeayne, A. R., Manke, D. R., and Baumann, M. H. (**2024**) Pharmacological profiles and psychedelic-like effects of 4-hydroxy-, 4-acetoxy-, and 4-methoxy-N- methyl- N- isopropyltryptamine, *The Journal of Pharmacology and Experimental Therapeutics 389*, 281, DOI: https://doi.org/10.1124/jpet.281.923160.
(67) Gessner, P. K., Khairallah, P. A., McIsaac, W. M., and Page, I. H. (**1960**) THE RELATIONSHIP BETWEEN THE METABOLIC FATE AND PHARMACOLOGICAL ACTIONS OF SEROTONIN, BUFOTENINE AND PSILOCYBIN, *The Journal of Pharmacology and Experimental Therapeutics 130*, 126-133, DOI: https://doi.org/10.1016/S0022-3565(25)25873-6.
(68) Toshihiro, T., Kazuhiro, T., Tatsuo, I., Kazuhiko, Y., Ren, I., Kiichi, I., and Shigeo, N. (**1985**) 11C-labelling of indolealkylamine alkaloids and the comparative study of their tissue distributions, *The International Journal of Applied Radiation and Isotopes 36*, 965-969, DOI: https://doi.org/10.1016/0020-708X(85)90257-1.
(69) Silva, M. T. A., and Calil, H. M. (**1975**) Screening hallucinogenic drugs: Systematic study of three behavioral tests, *Psychopharmacologia 42*, 163-171, DOI: 10.1007/BF00429548.
(70) Klein, A. K., Chatha, M., Laskowski, L. J., Anderson, E. I., Brandt, S. D., Chapman, S. J., McCorvy, J. D., and Halberstadt, A. L. (**2021**) Investigation of the Structure-Activity Relationships of Psilocybin Analogues, *ACS Pharmacol Transl Sci 4*, 533-542, DOI: 10.1021/acsptsci.0c00176.
(71) Tylš, F., Páleníček, T., Kaderábek, L., Lipski, M., Kubešová, A., and Horácek, J. (**2016**) Sex differences and serotonergic mechanisms in the behavioural effects of psilocin, *Behavioural Pharmacology 27*, 309-320, DOI: 10.1097/fbp.0000000000000198.

(72) Elmore, J. S., Decker, A. M., Sulima, A., Rice, K. C., Partilla, J. S., Blough, B. E., and Baumann, M. H. (**2018**) Comparative neuropharmacology of N-(2-methoxybenzyl)-2,5-dimethoxyphenethylamine (NBOMe) hallucinogens and their 2C counterparts in male rats, *Neuropharmacology 142*, 240-250, DOI: https://doi.org/10.1016/j.neuropharm.2018.02.033.
(73) Sherwood, A. M., Halberstadt, A. L., Klein, A. K., McCorvy, J. D., Kaylo, K. W., Kargbo, R. B., and Meisenheimer, P. (**2020**) Synthesis and Biological Evaluation of Tryptamines Found in Hallucinogenic Mushrooms: Norbaeocystin, Baeocystin, Norpsilocin, and Aeruginascin, *J Nat Prod 83*, 461-467, DOI: 10.1021/acs.jnatprod.9b01061.
(74) Glatfelter, G. C., Pottie, E., Partilla, J. S., Stove, C. P., and Baumann, M. H. (**2024**) Comparative Pharmacological Effects of Lisuride and Lysergic Acid Diethylamide Revisited, *ACS Pharmacology & Translational Science 7*, 641-653, DOI: 10.1021/acsptsci.3c00192.
(75) Kitagaki, M., and Hirota, M. (**2007**) Auricular Chondritis Caused by Metal Ear Tagging in C57BL/6 Mice, *Veterinary Pathology 44*, 458-466, DOI: 10.1354/vp.44-4-458.
(76) Lapp, H. E., Salazar, M. G., and Champagne, F. A. (**2023**) Automated maternal behavior during early life in rodents (AMBER) pipeline, *Scientific Reports 13*, 18277, DOI: 10.1038/s41598-023-45495-4.
(77) Popik, P., Cyrano, E., Piotrowska, D., Holuj, M., Golebiowska, J., Malikowska-Racia, N., Potasiewicz, A., and Nikiforuk, A. (**2024**) Effects of ketamine on rat social behavior as analyzed by DeepLabCut and SimBA deep learning algorithms, *Frontiers in Pharmacology 14*, DOI: 10.3389/fphar.2023.1329424.
(78) Halberstadt, A. L., Koedood, L., Powell, S. B., and Geyer, M. A. (**2011**) Differential contributions of serotonin receptors to the behavioral effects of indoleamine hallucinogens in mice, *J Psychopharmacol 25*, 1548-1561, DOI: 10.1177/0269881110388326.
(79) Halberstadt, A. L., and Geyer, M. A. (**2011**) Multiple receptors contribute to the behavioral effects of indoleamine hallucinogens, *Neuropharmacology 61*, 364-381, DOI: 10.1016/j.neuropharm.2011.01.017.
(80) Halberstadt, A. L. (**2015**) Recent advances in the neuropsychopharmacology of serotonergic hallucinogens, *Behav Brain Res 277*, 99-120, DOI: 10.1016/j.bbr.2014.07.016.
(81) Kane, G. A., Lopes, G., Saunders, J. L., Mathis, A., and Mathis, M. W. (**2020**) Real-time, low-latency closed-loop feedback using markerless posture tracking, *eLife 9*, e61909, DOI: 10.7554/eLife.61909.
(82) Ye, S., Filippova, A., Lauer, J., Schneider, S., Vidal, M., Qiu, T., Mathis, A., and Mathis, M. W. (**2024**) SuperAnimal pretrained pose estimation models for behavioral analysis, *Nature Communications 15*, 5165, DOI: 10.1038/s41467-024-48792-2.
(83) Kapoor, S., and Narayanan, A. (**2023**) Leakage and the reproducibility crisis in machine-learning-based science, *Patterns 4*, 100804, DOI: https://doi.org/10.1016/j.patter.2023.100804.
(84) Insafutdinov, E., Pishchulin, L., Andres, B., Andriluka, M., and Schiele, B. (**2016**) DeeperCut: A Deeper, Stronger, and Faster Multi-person Pose Estimation Model, In *Computer Vision – ECCV 2016* (Leibe, B., Matas, J., Sebe, N., and Welling, M., Eds.), pp 34-50, Springer International Publishing, Cham.
(85) He, K., Zhang, X., Ren, S., and Sun, J. (**2015**) Deep Residual Learning for Image Recognition, *arXiv [cs.CV]*.
(86) Schindler, C. W., Thorndike, E. B., Partilla, J. S., Rice, K. C., and Baumann, M. H. (**2021**) Amphetamine-like Neurochemical and Cardiovascular Effects of α-Ethylphenethylamine Analogs Found in Dietary Supplements, *J Pharmacol Exp Ther 376*, 118-126, DOI: 10.1124/jpet.120.000129.
(87) Glatfelter, G. C., Walther, D., Evans-Brown, M., and Baumann, M. H. (**2021**) Eutylone and Its Structural Isomers Interact with Monoamine Transporters and Induce Locomotor Stimulation, *ACS Chemical Neuroscience 12*, 1170-1177, DOI: 10.1021/acschemneuro.0c00797.
(88) Solis, E., Jr., Partilla, J. S., Sakloth, F., Ruchala, I., Schwienteck, K. L., De Felice, L. J., Eltit, J. M., Glennon, R. A., Negus, S. S., and Baumann, M. H. (**2017**) N-Alkylated Analogs of 4-

Methylamphetamine (4-MA) Differentially Affect Monoamine Transporters and Abuse Liability, *Neuropsychopharmacology 42*, 1950-1961, DOI: 10.1038/npp.2017.98.

TOC Graphic

Rapid, open-source, and automated quantification of the head-twitch response in C57BL/6J mice using DeepLabCut and Simple Behavioral Analysis

Alexander D Maitland[1], Nicholas R Gonzalez[1], Donna Walther[1], Francisco Pereira[2], Michael H Baumann[1], and Grant C Glatfelter[1*]

[1]Designer Drug Research Unit, National Institute on Drug Abuse, Intramural Research Program, Baltimore, Maryland

[2]Machine Learning Team, National Institute of Mental Health, Intramural Research Program, Bethesda, Maryland
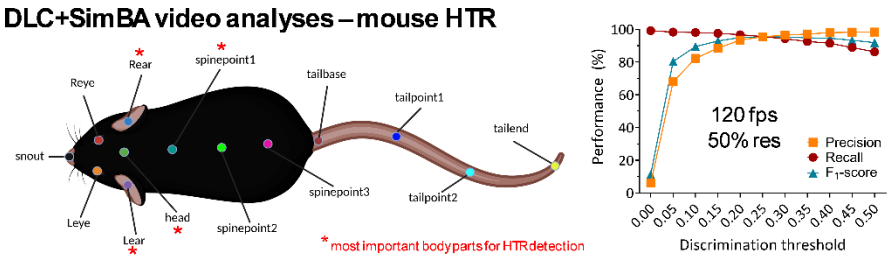
*Corresponding author: grant.glatfelter@nih.gov